Journal of
Manufacturing and Materials Processing

MDPI

Article

An Experimental Investigation into the Enhancement of Surface Quality of Inconel 718 Through Axial Ultrasonic Vibration-Assisted Grinding in Dry and MQL Environments

Sreethul Das [1], Pandivelan Chinnaiyan [1], Joel Jayaseelan [1], Jeyapandiarajan Paulchamy [1], Andre Batako [2,*] and Ashwath Pazhani [3]

[1] School of Mechanical Engineering, Vellore Institute of Technology, Vellore 632014, India; sreethuldas@vit.ac.in (S.D.); cpandivelan@vit.ac.in (P.C.); joel.j@vit.ac.in (J.J.); jeyapandiarajan.p@vit.ac.in (J.P.)
[2] General Engineering Research Institute, Liverpool John Moores University, Liverpool L3 5UX, UK
[3] Faculty of Engineering, Environment and Computing, Coventry University, Coventry CV1 5FB, UK; ae0255@coventry.ac.uk
* Correspondence: a.d.batako@ljmu.ac.uk

Abstract: Ultrasonic vibration-assisted grinding (UVAG) has proven to be beneficial for grinding difficult-to-machine materials. This work attempts to enhance the grinding performance of Inconel 718 through a comprehensive study of UVAG characteristics. Grinding experiments were performed in both dry and Minimum Quantity Lubrication (MQL) environments, and assessment of the grinding forces, specific energy, residual stress, and surface topography was done. A substantial reduction of both surface roughness and grinding force components was observed in UVAG compared to conventional grinding (CG). Utilizing UVAG with MQL at the maximum vibration amplitude led to a 64% reduction in tangential grinding force and a 51% decrease in roughness parameter, R_a, when compared to CG conducted in a dry environment. The high-frequency indentations of the abrasives in UVAG generated compressive residual stresses on the ground surface. Surface parameters pointed to uniform texture and SEM images showed widening of abrasive grain tracks on the workpiece surface during UVAG. The utilization of UVAG under MQL produced a synergistic impact and resulted in the lowest grinding forces, specific energy, and optimal surface quality among all the grinding conditions investigated. Overall analysis of the results indicated that the axial configuration of the vibration set-up is favorable for UVAG, and the high-frequency periodic separation-cutting characteristic of the process improves lubricating efficiency and grinding performance.

Keywords: hybrid machining; axial UVAG; Inconel 718; surface texture; residual stress; MQL; synergistic effect

Citation: Das, S.; Chinnaiyan, P.; Jayaseelan, J.; Paulchamy, J.; Batako, A.; Pazhani, A. An Experimental Investigation into the Enhancement of Surface Quality of Inconel 718 Through Axial Ultrasonic Vibration-Assisted Grinding in Dry and MQL Environments. *J. Manuf. Mater. Process.* **2024**, *8*, 255. https://doi.org/10.3390/jmmp8060255

Academic Editor: Alborz Shokrani

Received: 25 September 2024
Revised: 28 October 2024
Accepted: 4 November 2024
Published: 13 November 2024

1. Introduction

Inconel 718 has widespread applications in various sectors due to its excellent mechanical and physical properties [1,2]. However, issues related to its machinability still pose several challenges, and it is subject to widespread research [3–5]. Conventional grinding (CG) of Inconel 718 often results in poor surface quality due to high grinding force, surface burns, tensile residual stress, and tool wear [6–8]. Even though the use of cooling and lubrication systems is deemed effective, researchers are exploring sustainable alternatives such as MQL and hybrid machining processes for efficient machining of difficult-to-machine materials. Hybrid machining is gaining momentum due to its synergistic effects on machining characteristics and its capability to improve the process in an environmentally sustainable manner [9–11]. Ultrasonic vibration-assisted grinding (UVAG or UAG) is a hybrid grinding process in which high-frequency vibration is imparted to the grinding zone (through the tool or workpiece), which alters the monotonous abrasive–workpiece interaction in conventional grinding (CG) to an intermittent separation–cutting process.

This has proven to create a separation phase of the abrasive from the workpiece and alter the chip formation, which lowers the grinding force, temperature, and tool wear, leading to improvement of the surface quality [12,13].

Vibration-assisted grinding experiments on Inconel 718 carried out by Ibrahim et al. [14] recorded a reduction of grinding forces, lower surface roughness, and increased material removal compared to CG. A comparative study of grinding performance on single crystal turbine blade tenons performed at different conditions outlined several beneficial features of UVAG [15]. The study highlights the role of superposition of abrasive grain traces during UVAG in the generation of uniform, shallow scratches on the surface, thereby improving the surface properties when compared with CG. Tawakoli et al. [16] reported that UVAG has the potential to reduce heat generation and lower the grinding forces and profile loss of the grinding wheel. They also found that grinding force and surface roughness are lower in UVAG. Li et al. [17] investigated the capabilities of UVAG for improving the grinding characteristics of Inconel 718. The effects of vibration amplitude, depth of cut, and wheel rotational speed on material removal, surface roughness, and grinding force in dry grinding conditions were studied. Ultrasonic vibration assistance during grinding was found to be beneficial in reducing forces while grinding Inconel 718. Changes in chip morphology as a result of superimposed vibrations were found to be responsible for the reduction of grinding forces during UVAG. Minimum quantity lubrication (MQL) is a lubrication strategy in which a small quantity of lubricant is introduced to the cutting zone in an atomized form using pressurized air. This is considered as an environmentally friendly alternative, as it facilitates near-dry machining. Researchers have employed MQL during UVAG for steel alloys and have observed enhancement in the lubrication effect due to the presence of high-frequency vibrations [18,19].

Hence, UVAG has immense potential in overcoming the challenges associated with grinding of difficult-to-machine materials. However, this has not been utilized adequately for investigating the grindability of Inconel 718. In this study, a comparative assessment of residual stresses, microhardness, roughness parameters, surface topography, and SEM images of the ground surface of Inconel 718 under various conditions was performed.

2. Materials and Methods

The experimental set-up utilized for UVAG consists of an ultrasonic vibration system integrated with a surface grinding machine, as shown in Figure 1. The ultrasonic system consists of a power supply, generator/control unit system, converter, and horn/sonotrode. The ultrasonic generator is responsible for converting standard electrical power into high-frequency oscillating signals. The generator used here has a power rating of 1800 W and features the control unit. A rotary switch in the control unit is used to set the vibration amplitude to four levels, whereas the frequency of vibration remains fixed at 19.8 kHz during the operation. In an ultrasonic stack assembly, the section which houses the piezo-electric crystal is known as the converter. The converter is connected to the booster, which transmits the vibrations to the sonotrode. The oscillating current is converted to mechanical vibrations using the piezoelectric transducer. The vibrations are amplified by the booster and transmitted to a rectangular horn/sonotrode on which the workpiece is mounted. The block sonotrode rests on top of a supporting base, which has needle rollers embedded on the top surface that allow it to vibrate freely with minimal energy losses. The supporting fixtures for the stack assembly and sonotrode are mounted on the dynamometer fixed on the grinding table, using a base plate. Further details on the design and configuration of the experimental set-up can be found in a previous work by Das et al. [20]. The schematic of the experimental set-up ultrasonic stack assembly and fixtures mounted on a dynamometer and its orientation with respect to the grinding parameters is shown in Figure 2.

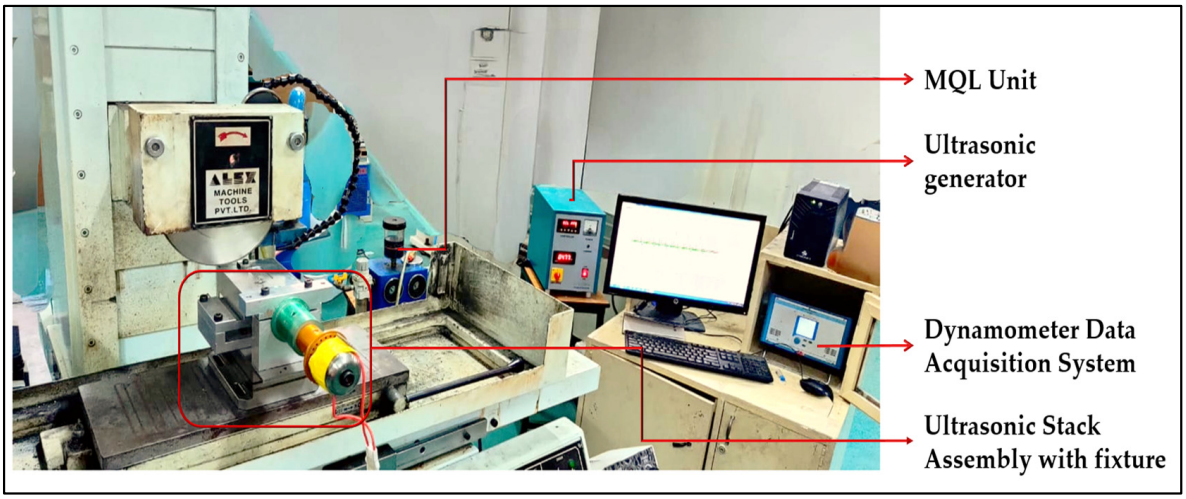

Figure 1. UVAG set-up with ultrasonic stack assembly unit and data acquisition system.

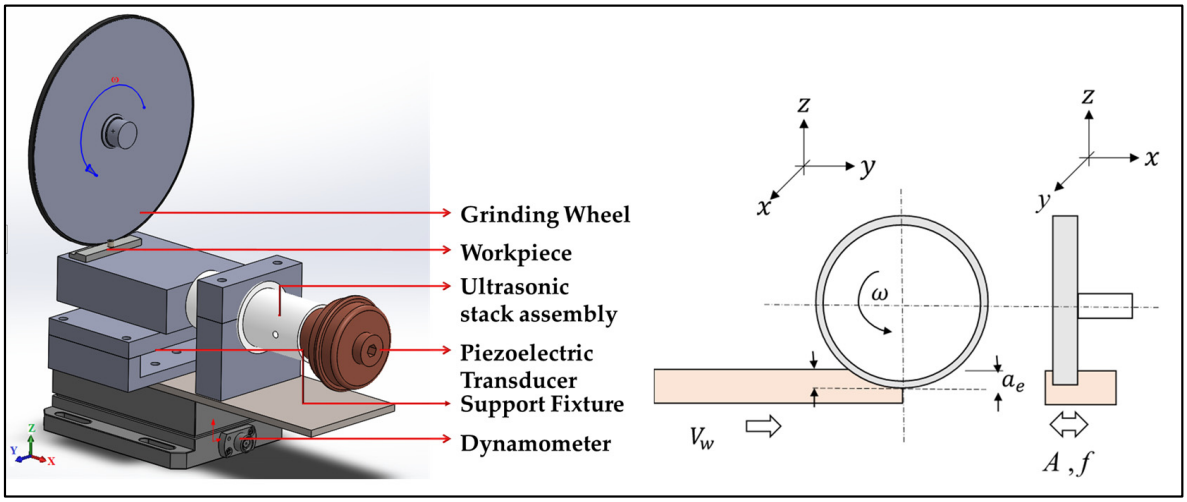

(**a**) (**b**)

Figure 2. (**a**) Schematic of ultrasonic stack assembly and fixtures mounted on dynamometer. (**b**) Schematic of UVAG parameters with respect to the grinding wheel.

While designing the experiments, careful consideration was given to the configuration of the experimental set-up and the impact of various parameters on grinding performance. These aspects are discussed in detail below.

The process kinematics of UVAG require a critical condition to be satisfied during parameter selection to ensure tool–workpiece disengagement in UVAG [21,22] when vibrations are applied parallel to the feed direction. This condition, given by equation 1, dictates that specific parameter combinations of workpiece speed (V_w), vibration amplitude (A), and frequency (f) must be maintained to ensure separation–cutting characteristics in UVAG.

$$V_w < 2\pi Af \tag{1}$$

Increasing parameters like cutting speed or feed rate beyond optimal levels can disrupt this balance and hinder tool–workpiece disengagement in UVAG. Consequently, this diminishes the ability of vibrations to enhance the cutting action and lowers productivity due to reduced material removal rate. However, when vibrations are applied perpendicular to the feed direction, there is always tool–workpiece disengagement satisfying the requirement of vibratory grinding [14]. Considering this, an axial UVAG configuration is adopted where the ultrasonic vibrations are provided to the workpiece perpendicular

to the feed direction. The grinding forces and temperature in grinding increase with an increase in workpiece speed and grinding depth (a_e), which can severely degrade surface quality. Moreover, higher values of feed rate and depth of cut tend to diminish the effectiveness of ultrasonic vibrations in UVAG [23]. Based on these considerations, the depth of cut and workpiece speed were selected and maintained at constant low values based on our previous study [24] throughout all experiments, to ensure optimal performance and surface quality.

In contrast, an increase in peripheral wheel speed (V_c) reduces the chip thickness in grinding, thereby lowering the grinding forces and temperature [25]. Therefore, the wheel speed is kept at the maximum value in the operating range. This study focuses on the effects of vibration amplitude, which is varied using the ultrasonic controller. The vibration amplitude is varied within the operational range of the ultrasonic controller, enabling us to assess its influence on grinding performance under both dry and MQL conditions. In conclusion, the experimental configuration and parameter selection were designed to ensure that, while assessing the impact of UVAG, other parameters were kept at levels that facilitated clear interpretation of the results. Overall, the experimental design provides a controlled environment that highlights the benefits of ultrasonic assistance on grinding.

Grinding experiments were performed on an Inconel 718 workpiece measuring 100 mm × 20 mm × 10 mm. Details of the grinding wheel and other process conditions used for experimentation are given in Table 1. The grinding forces were recorded using a Kistler 9257B dynamometer (Manufacturer: Kistler Instrumente AG, Winterthur, Switzerland) interfaced with Dynoware software Version 3.3.2.0. A Vicker's hardness tester was used to measure the microhardness values, and a μ-X360 residual stress tester (Manufacturer: Xstress GmbH, Stuttgart, Germany) employing the Debye ring method was used to measure the surface residual stress. The 2D surface roughness parameters were measured using a MarSurf GD 120 roughness measurement system (Manufacturer: Mahr GmbH, Göttingen, Germany). For each sample, the roughness values were measured at five locations perpendicular to the grinding direction, and the average values have been noted. Scanning electron microscope (SEM) images captured using a JEOL JCM-6000 Benchtop SEM (Manufacturer: JEOL Ltd., Tokyo, Japan) were used to compare the surface characteristics of ground samples. The 3D surface texture was captured using a Talysurf CCI 3000 non-contact 3D surface profiler (Manufacturer: Taylor Hobson, a subsidiary of Ametek, Inc., Leicester, United Kingdom) with a magnification of 50×, numerical aperture of 0.55, and a lateral sampling resolution of 0.36 μm, over a measurement field of 1.8 mm × 1.8 mm. The system makes use of Taly Map Platinum 5.1.1.5374 software to obtain three-dimensional surface profiles and roughness parameters. The images of multiple measurements were stitched together to create a comprehensive representation of the topography. In the processing of the 3D images, the original surface was levelled to remove large-scale variations, followed by the application of a high-pass filter with a cut-off frequency of 0.025 mm.

Table 1. Experimental conditions and process parameters.

Specifications	Details	
Grinding wheel	Metal bonded wheel, cBN abrasive Diameter (D)—200 mm, wheel width (B)—10 mm Mesh size #100/120	
Processing parameters	Vibration amplitude (A) Wheel speed (V_c) Depth of cut (a_e) Workpiece speed (V_w)	14, 16, 18, 20 μm 30 m/s 10 μm 19 m/min
MQL parameters	Cutting fluid Oil flowrate Air pressure	Neat oil 100 mL/h 6 bars

3. Results

The analysis of the experimental results is provided in the following sections:

3.1. Grinding Force

The normal (F_n) and tangential (F_t) grinding forces for grinding experiments carried out in dry and MQL environments are plotted in Figure 3. CG recorded the highest value of force components in both dry and MQL environments. It is clear from Figure 3 that grinding in presence of ultrasonic vibration lowered the grinding force components irrespective of the grinding condition. The overlapping of abrasive grain traces in UVAG is reported to reduce the chip cross sectional area [26], which results in lower forces in UVAG. As expected, the grinding forces consistently reduced as the amplitude of vibration increased. In dry grinding, it is observed that the F_t and F_n values reduced by 33% and 27%, respectively, in UVAG at the highest vibration amplitude (20 µm). MQL is able to significantly reduce the grinding forces in CG and UVAG through the Rehbinder effect [27].

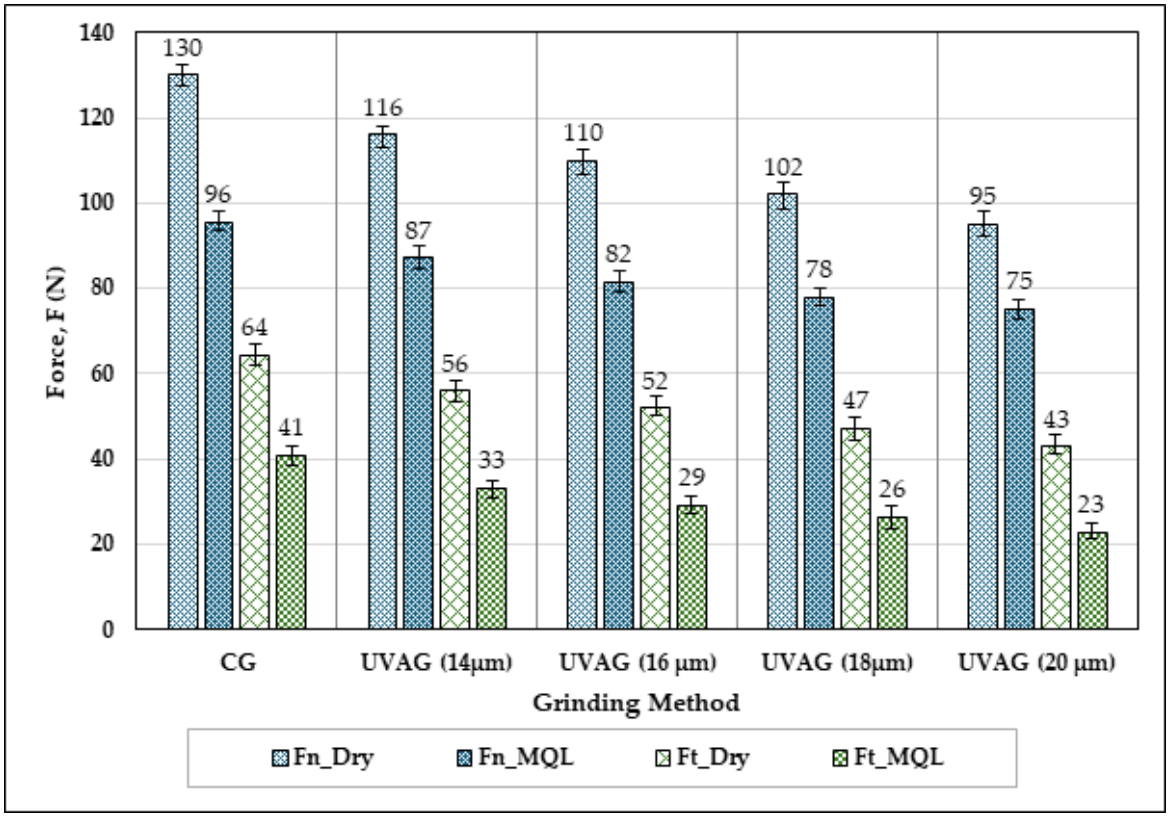

Figure 3. Comparison of normal (F_n) and tangential (F_t) grinding forces in CG and UVAG (at different amplitude levels) for dry and MQL conditions.

When grinding was performed in MQL in UVAG at 20 µm amplitude, the F_t and F_n values were lowered by 44% and 22%, respectively, when compared to MQL in CG, indicating that the effectiveness of MQL is increased in the presence of the ultrasonic vibrations provided in UVAG. The periodic separation characteristic between the abrasive grains and workpiece enhanced lubrication through effective lubricant penetration to the cutting zone, which enabled reduction of grinding forces when UVAG was performed under MQL conditions. An overall reduction of F_t and F_n by 64% and 42%, respectively, was realized when UVAG with MQL was adopted as compared to CG under dry conditions, which is a significant reduction. Similar reductions of grinding forces have been reported in the literature [17,18] by adopting MQL in UVAG.

From the mechanics of the process, the equations of motion of a single abrasive relative to the workpiece in the horizontal plane ($x - y$) in UVAG can be written as follows. The axial motion of an abrasive can be expressed as:

$$x(t) = A\ sin(2\pi ft) \tag{2}$$

Considering the workpiece movement in the tangential direction (y direction) and the rotation of grinding wheel, the relative motion of abrasive in the table feed direction (y direction) may be expressed as:

$$y(t) = V_\omega t + (D/2 \times sin(2\pi N_s t)) \tag{3}$$

$$z(t) = D/2cos(2\pi N_s t) \tag{4}$$

where A: vibration amplitude, f: vibration frequency, D: wheel diameter, and N_s: wheel speed in rps.

The path of a single abrasive as per Equations (2)–(4) can be visualized as shown in Figure 4. The path of abrasive grit in CG is also shown for comparison. From the figure, it can be seen that the abrasive grit traces an elliptical path over the workpiece in UVAG as opposed to the monotonous circular path traced in CG.

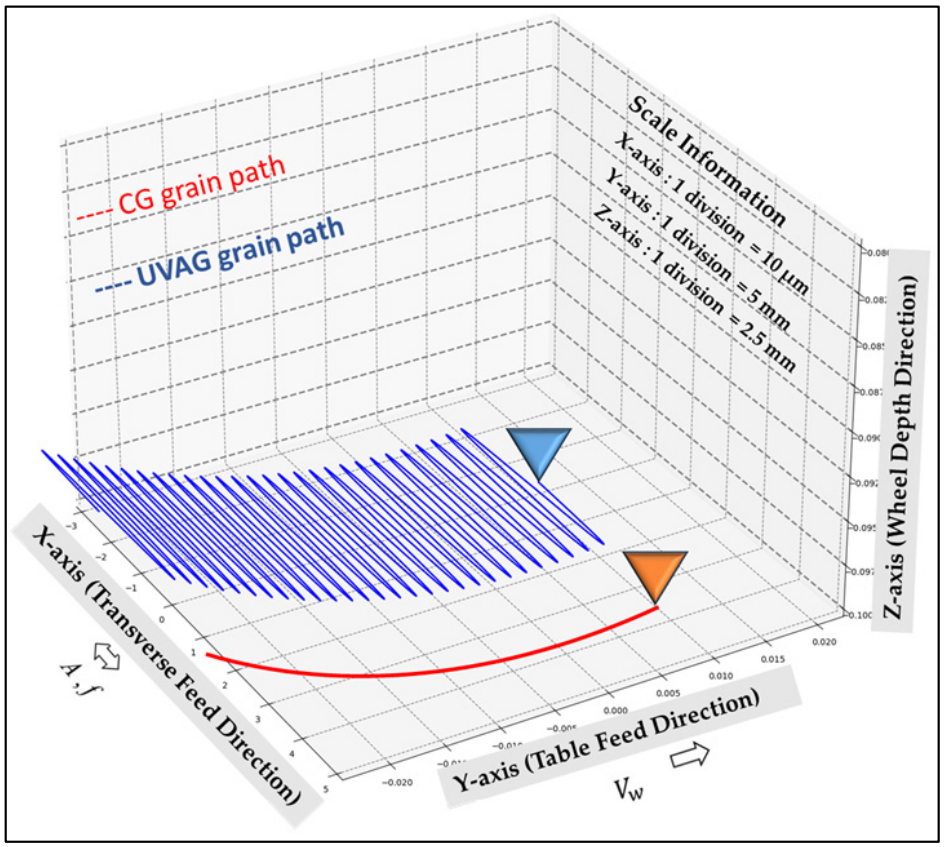

Figure 4. Visualization of path traced by an abrasive grit relative to the workpiece surface in CG and UVAG (A = 20 µm, f = 19.8 kHz, V_w = 19 m/min, N = 2900 rpm and D = 200 mm).

Equations (2) and (3), when differentiated with respect to time (t), give the velocity components in the $x - y$ plane:

$$V_x = 2\pi fA\ cos(2\pi ft) \tag{5}$$

$$V_y = V_w + V_c\ cos(2\pi N_s t) \tag{6}$$

Here, V_x (axial velocity) corresponds to the abrasive motion along the transverse feed direction in the presence of ultrasonic vibration, and V_y is velocity component along the wheel rotation in UVAG. The cutting dynamics in UVAG are hence different from those of CG due to the elliptical cutting motion of the abrasive, which gives rise to overlapping grain traces over the workpiece surface during the grinding process. Equation (4) implies the cutting action of abrasives due to motion in the axial direction. This periodic motion is responsible for the enhancement of the cutting and separation machining characteristics of abrasives in axial UVAG. The elliptical motion of abrasives enhances the contact area between the abrasives and the workpiece, thereby increasing material removal in axial UVAG. This can be confirmed from the force component F_x recorded by a dynamometer. The velocity V_x calculated using Equation (4) and F_x are plotted in Figure 5. F_t is also shown for comparison.

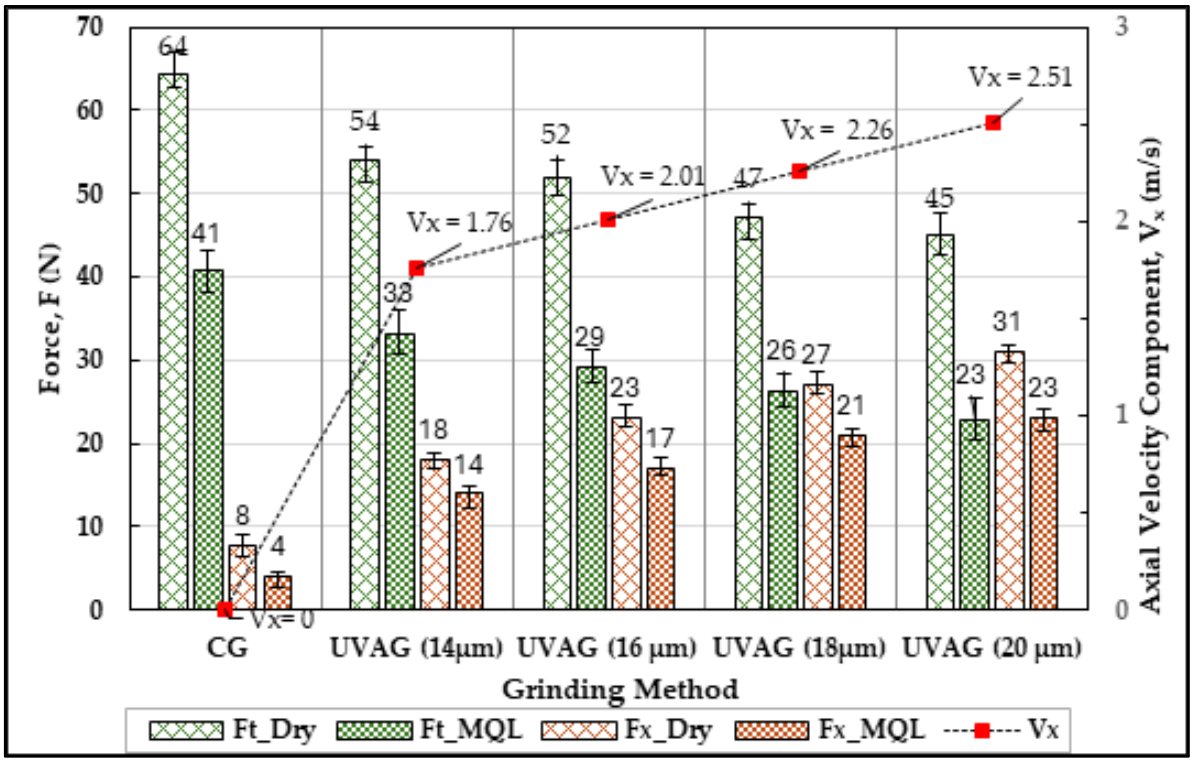

Figure 5. Tangential force F_t, axial force F_x, and axial velocity V_x components of UVAG (at different amplitude levels) in dry and MQL environments.

It can be observed that the magnitude of F_x increases as the vibration amplitude increases, and at higher vibration amplitudes the values are comparable to F_t. The force component F_x arises from the high-frequency vibrations during axial ultra-precision abrasive grinding (UVAG). Consequently, this can be regarded as contributing to the self-sharpening of grinding wheels, attributed to the periodic impact action in the transverse direction. This self-sharpening action of grinding wheels has been pointed out in the literature to enhance grinding performance in UVAG [28,29]. As the magnitude of F_x and V_x increases with increased vibration amplitude, the lower grinding forces at higher amplitudes can be associated with this characteristic in UVAG.

3.2. Coefficient of Friction (μ) and Specific Energy (u)

The coefficient of friction (μ), which is the ratio of F_t to F_n, is an important parameter in grinding that influences the specific energy and heat generation at the work surface. μ is an indicator of the energy required and the ease of material removal during the grinding process. A low value of μ in grinding indicates lesser ploughing action and efficient cutting of abrasive grains [30].

From Figure 6 it is observed that the μ value is consistently lower in UVAG for both dry and MQL conditions The lower value of μ observed in UVAG compared to CG highlights efficient cutting action of the abrasives in UVAG. It is also notable that the μ value reduces as the vibration amplitude increases during UVAG in both dry and MQL conditions. Under MQL conditions, the presence of lubricant film around the abrasives facilitates slipping between the grits and workpiece, which lowers friction [31]. UVAG with MQL was found to have a lower μ when compared with CG with MQL. This is due to enhanced lubrication resulting from abrasive–workpiece disengagement in the presence of superimposed vibrations, which enables effective penetration of lubricant to the grinding zone. Thus, the presence of vibration enhances lubrication, which produces a synergistic effect during the grinding process. Also, a lower value of μ can result in compressive residual stress distribution on the ground surface [30] which is favorable for fatigue life of ground components. Furthermore, a low value of μ is associated with lower tangential cutting force and low specific energy, which has a favorable influence on the surface quality [32].

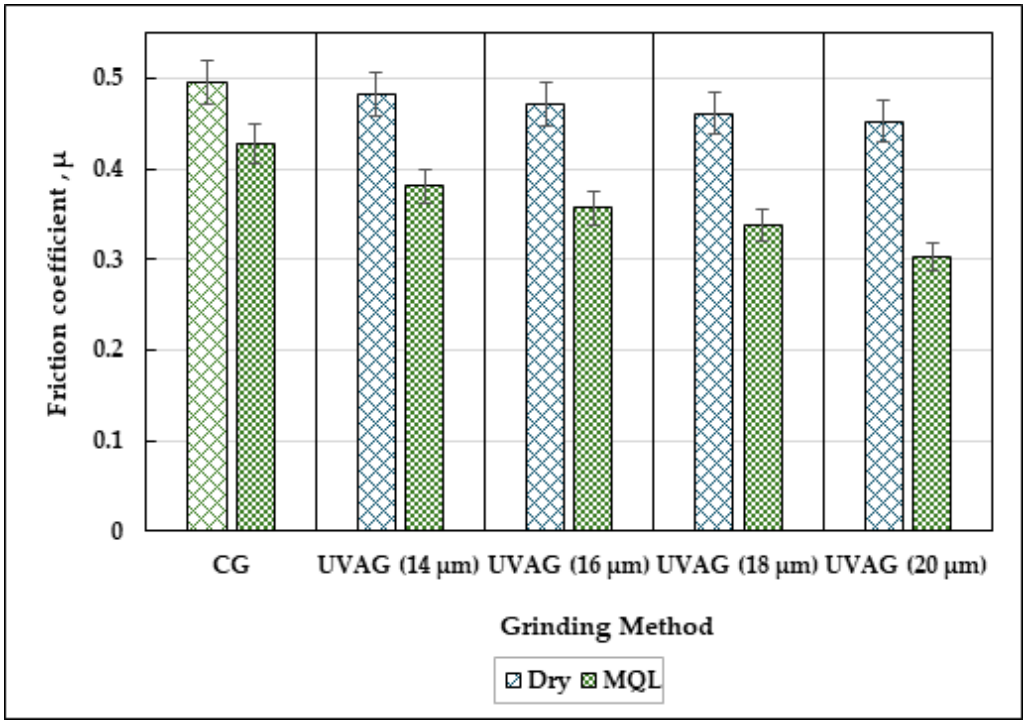

Figure 6. Coefficient of friction (μ) in UVAG under dry and MQL conditions at different vibration amplitudes.

The energy required for unit volume removal of material is known as specific energy (U). Due to the presence of undesirable plowing and sliding action of abrasive grits, the specific energy in grinding operations is high. A lower value of specific energy in grinding indicates efficient cutting action of abrasives by lowering the contribution of plowing and rubbing effects, which are responsible for heat generation.

Specific energy values for CG (U_{CG}) and UVAG (U_{UVAG}) are calculated using Equations (7) and (8), as follows:

$$U_{CG} = (F_t \times V_c)/(B \times a_e \times V_w) \quad (7)$$

$$U_{UVAG} = [(F_t \times V_c) + (F_x \times V_x)]/(B \times a_e \times V_w) \quad (8)$$

where U_{CG} and U_{UVAG} denote the specific energy in CG and UVAG, respectively, in terms of tangential grinding force and grinding parameters.

The calculation of specific energy in UVAG (Equation (8)) considered the cutting action in the axial direction as well. Specific energy values at different vibration amplitudes are

plotted Figure 7. The values in CG are also given for comparison. The specific energy was observed to reduce as the vibration amplitude increased, which indicates higher material removal efficiency in UVAG. As pointed out earlier, the sharper grains in UVAG improve the cutting action of grains, as opposed to the undesirable sliding action. This reduces the grinding forces and thereby lowers the specific energy in UVAG, enhancing the efficiency of material removal in UVAG. The reduction of specific energy in UVAG denotes lowering of undesirable thermal effects, which is expected to improve the surface quality [33].

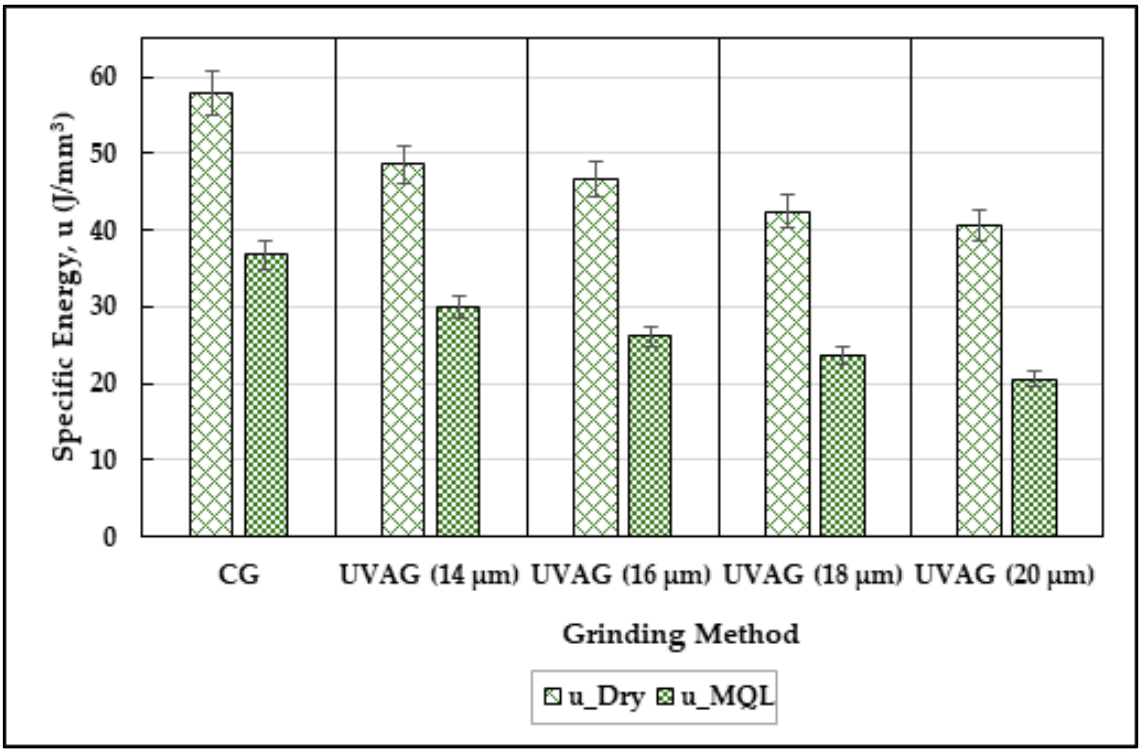

Figure 7. Specific energy in UVAG under dry and MQL conditions at different vibration amplitudes.

3.3. Residual Stress and Microhardness

In the grinding process, the loading induced by abrasive grits on the workpiece is thermo-mechanical in nature. Depending on the predominant load existing on the workpiece during material removal, the resulting surface may possess favorable or unfavorable mechanical properties. Predominance of thermal load can lead to tensile residual stress or microstructural transformations, which may increase the surface hardness or induce surface cracks. However, the predominance of mechanical loading of abrasive grains on the workpiece surface induces compressive residual stress, which can be considered as a desirable effect from a fatigue loading perspective [34]. Figure 8 shows the residual stress measured at the surface for samples processed with CG and UVAG. It can be seen that residual stress is in the compressive range for all samples. The combined effect of high thermal conductivity and hardness of the CBN wheels removes the heat generated during grinding and results in compressive residual stresses [35]. As the vibration amplitude increases, the compressive stress on the surface can also be seen to increase. The high-frequency vibrations in UVAG result in a peening effect of abrasive grits on the workpiece surface. This imposes an additional mechanical load on the workpiece, thereby resulting in generation of compressive stress on the workpiece surface [36]. Also, periodic separation of the abrasive during engagement with the workpiece surface in UVAG results in effective dissipation of the heat generated. This ensures that the loading nature on the workpiece surface is predominantly mechanical, as opposed to thermal loads induced by heat generation. As discussed earlier, the lower coefficient of friction in vibration-assisted grinding also favors the generation of compressive stress. The contribution of axial vibration to

determining the stress response needs to be noted here. The presence of ultrasonic vibration in an axial/transverse direction leads to the movement of abrasives in the axial direction, creating an elliptical trace on the workpiece surface. This leads to increased contact area of the abrasive over the workpiece. However, in the absence of ultrasonic vibration, the abrasive grain traces a linear path over the workpiece. Through an experimental work on grinding of Inconel 718, it was inferred by Curtis et al. [8] that conditions of lower contact length and cutting speeds restrict heat transfer from the workpiece to the grinding wheel, which leads to tensile residual stress profiles. They further stated that the residual stress can be maintained in the compressive range by managing the portion of the total grinding heat imparted to the workpiece and the contact length during grinding. In UVAG, as the vibration amplitude increases, the axial velocity component and the contact area increase. Due to these factors, the contribution of ultrasonic vibration assistance towards efficient heat dissipation and the formation of compressive residual stress on the workpiece surface can be clearly inferred.

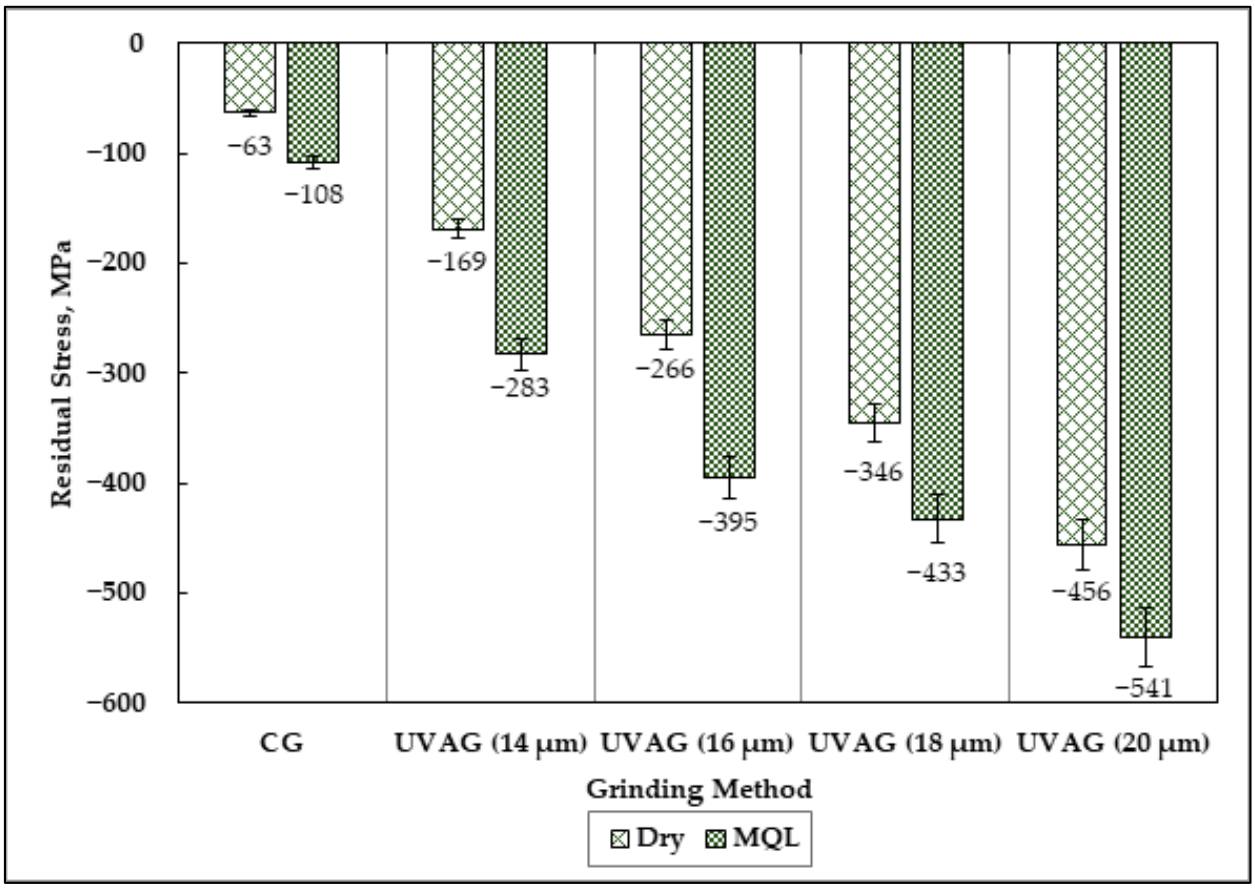

Figure 8. Surface residual stress in UVAG under dry and MQL conditions at different vibration amplitudes.

Application of MQL results in the removal of grinding heat and favors the generation of compressive residual stress. An experimental study on grinding of Inconel 718 showed that MQL using neat oil is effective for the removal of heat generated at the grinding zone, and the mechanical action of grits on the workpiece is enhanced [37]. The presence of pressurized air in MQL lowers wheel loading, which is also favorable for the generation of compressive residual stresses. When MQL is employed in UVAG, the lubricant effectively penetrates into the gap between the abrasive and workpiece due to disengagement of contact. This enhances the efficiency of lubrication through removal of the heat generated due to grinding, leading to a synergistic effect. As the amplitude of vibration is increased, the magnitude of compressive stress measured on the surface is found to increase. The vibration amplitude has a beneficial effect on residual stress, as observed from Figure 8,

and grinding performed in MQL at a vibration amplitude of 20 µm resulted in compressive residual stress of -541 ± 35 MPa.

Microhardness measurements can provide quantitative data on the mechanical properties of the material post-grinding, allowing us to assess the effectiveness of UVAG. Measuring microhardness allows for a correlation between hardness changes and the presence of compressive residual stresses induced by grinding. The microhardness values of the ground specimens are plotted in Figure 9. An increase in hardness values is expected after grinding due to the strain-hardening nature of Inconel 718 [38]. UVAG promotes dislocation formation, leading to strain hardening and surface strengthening, all while effectively maintaining lower grinding temperatures [39]. While compressive residual stresses enhance material performance by hindering dislocation movement, vibration also increases dislocation density through enhanced deformation, contributing to work hardening. In UVAG, the increase in microhardness arises from higher dislocation density resulting from plastic deformation, which enhances resistance to deformation by creating obstacles that impede dislocation movement. This interaction suggests that UVAG not only enhances surface hardness but also fosters beneficial stress states that improve fatigue and wear resistance. Strain hardening was facilitated by the high-frequency peening action and mechanical loading of abrasive grits in UVAG. The combination of strain hardening and compressive residual stresses in the samples was the result of predominant plastic deformation due to the mechanical action of the grits, along with the absence of thermal softening effects on the workpiece surface [40,41]. Additionally, the implementation of MQL further enhanced these effects. When combined with ultrasonic vibration, MQL amplified the benefits by improving lubrication and heat removal, facilitating controlled plastic deformation. This synergy ultimately led to enhancements in microhardness and compressive residual stresses.

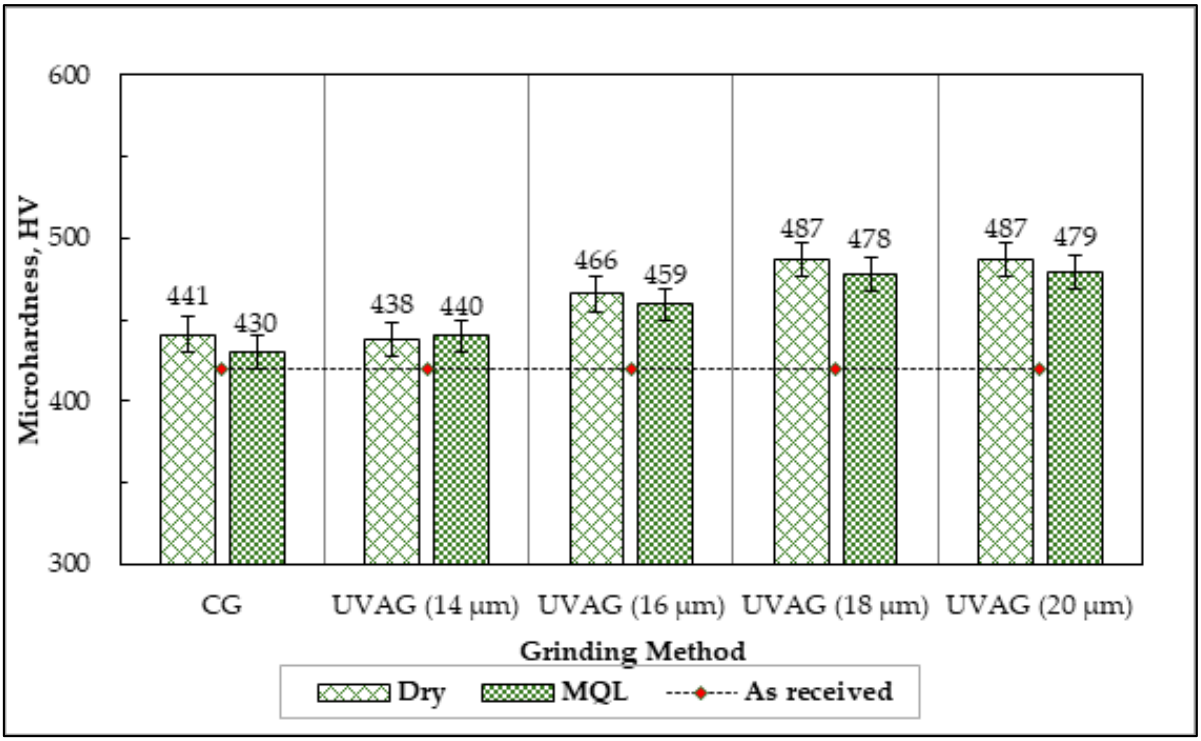

Figure 9. Microhardness of the samples from UVAG under dry and MQL conditions at different vibration amplitudes.

3.4. Surface Roughness and 3D Topography

Figure 10 shows the variation of average surface roughness (R_a) values for the samples ground under dry and MQL conditions. It can be observed that, as the vibration amplitude

is increased in UVAG under dry conditions (UVAG_Dry), the R_a value is consistently reduced from the CG value under dry conditions (CG_Dry). R_a reduces significantly when MQL is employed in UVAG (UVAG_MQL), and the effect is enhanced as the vibration amplitude is increased to 20 µm. There is a significant reduction of R_a, by almost 51%, when grinding is performed in UVAG_MQL at a 20 µm amplitude, the highest amplitude setting, as compared to CG_Dry. Grinding performed at 20 µm showed the highest improvement in terms of the parameters discussed in the previous sections. Henceforth, samples ground using UVAG at 20 µm will be used for comparison with those obtained through CG to examine variations in the surface texture. The assessment of surface profiles using 3D roughness parameters for samples obtained through UVAG at 20 µm under dry and MQL conditions with those in CG is given in Table 2.

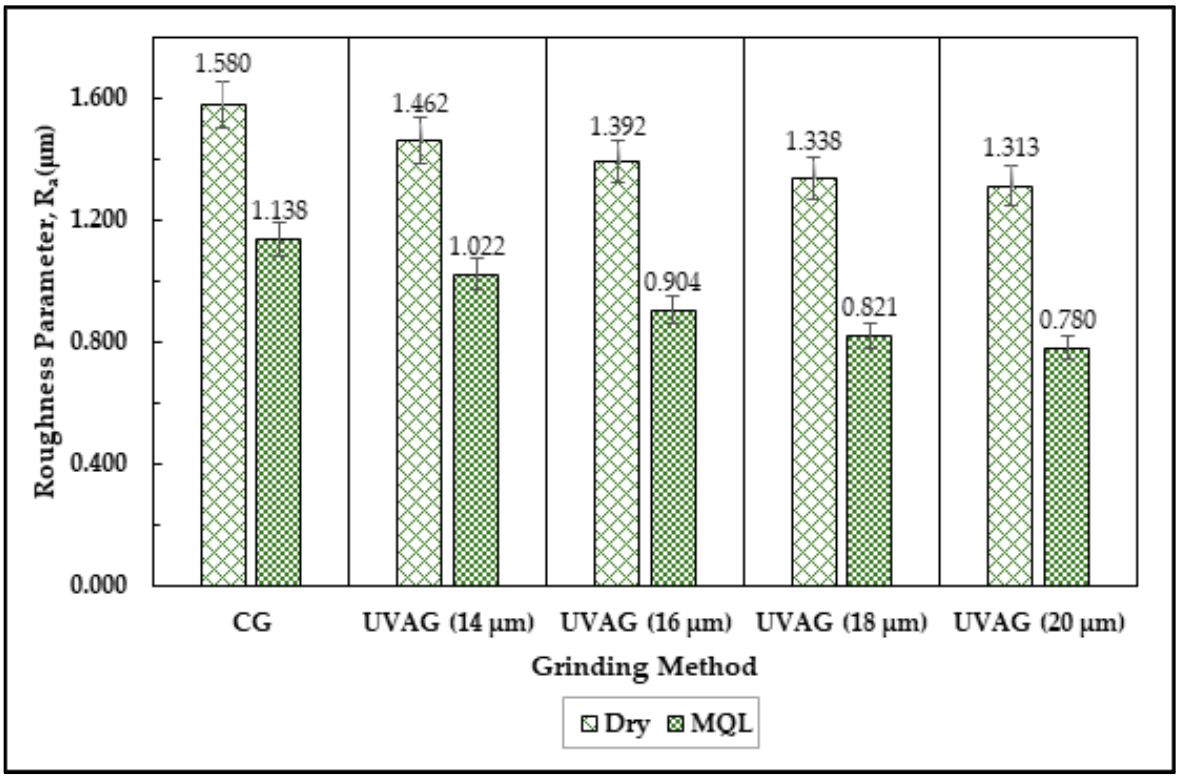

Figure 10. Plot of R_a values for dry and MQL grinding conditions in CG and UVAG.

Table 2. Comparison of 3D roughness parameters for CG and UVAG (A = 20 µm).

3D Surface Roughness Parameters	CG_Dry	UVAG_Dry	CG_MQL	UVAG_MQL	Unit
S_a	2.150	1.510	1.691	1.225	µm
S_q	2.719	1.907	2.333	1.692	µm
S_p	12.430	11.263	8.934	6.481	µm
S_v	10.142	7.552	8.942	8.226	µm
S_z	22.572	18.815	17.876	14.707	µm
S_c	5.905	4.814	4.013	3.161	µm
Ssk	−0.025	−0.167	−0.489	−0.256	
Sku	4.105	2.864	3.961	2.668	

Analysis of the surface roughness data revealed significant improvements when transitioning from conventional grinding (CG) to ultrasonic vibration-assisted grinding (UVAG), as well as from dry to minimum quantity lubrication (MQL) conditions. Both the average roughness (S_a) and the root mean square roughness (S_q) exhibited marked reductions in UVAG conditions compared to CG, indicating a smoother surface finish. Additionally, the maximum peak height (S_p) and maximum valley depth (S_v) were lower in UVAG processes, suggesting a more uniform texture with reduced surface irregularities. In contrast, the higher values of S_a and S_q in CG reflect greater surface irregularities compared to those obtained with UVAG. MQL conditions yield better surface finishes than dry conditions across both grinding methods, with the UVAG_MQL scenario achieving the lowest roughness values. However, it is notable that the roughness parameters values for UVAG_Dry were comparable to those for CG_MQL. This shows that the effectiveness of UVAG under dry conditions is comparable to UVAG with proper selection of parameters. A similar observation made by Gu et al. in their study [42] supports this result. From an ecological standpoint, this observation has significant advantages. This points at the potential reduction in lubricant usage due to effective grinding in UVAG_MQL, which not only lowers the environmental impact associated with lubricant disposal but can also contribute to a more sustainable manufacturing process.

Skewness (Ssk) values indicate a shift in surface texture, with UVAG processes exhibiting negative skewness, which may benefit applications requiring reduced friction. Furthermore, kurtosis (Sku) values demonstrate that UVAG leads to a more uniform surface texture with fewer sharp peaks, enhancing smoothness and performance. A Sku value below 3, coupled with a negative Ssk, suggests a plateaued surface with a sparse distribution of sharp peaks [43]. The distinctive feature of UVAG when compared with CG is the impact action and overlapping trajectory of abrasives due to high-frequency axial vibrations. Additionally, UVAG effectively reduces troughs in the surface texture along the grinding direction [12]. The surfaces produced through UVAG in this study exhibit this same characteristic. Overall, the results indicate the effectiveness of UVAG and MQL in improving the surface quality of Inconel 718. The observed enhancement in terms of 3D roughness parameters indicates a more uniform surface finish, which is essential for high-performance applications.

Figure 11 shows the comparison of 3D surface texture and SEM images of the ground surface. The ploughing marks and deep grooves are clearly visible in the sample obtained through CG in dry environment (Figure 11a). An uneven profile and material re-adhesion can also be observed in the SEM image. The 3D surface image also shows an uneven profile. The material which gets laterally displaced due to ploughing action gets thermally softened and reattached to the workpiece surface due to subsequent contact with abrasives [37]. Even though the surface texture shows improvement in an MQL environment, the predominance of ploughing marks on the surface are evident for the CG_MQL samples, as can be observed in Figure 11g. However, the SEM images (Figure 11d,j) and 3D plots (Figure 11f,l) reveal significant enhancement of surface texture and lowering of ploughing marks for samples obtained through UVAG. The wide uniform grinding tracks are due to an increase in abrasive contact area due to overlapping grain trajectories. The distinguishing feature between UVAG and CG is the separation of contact between the abrasives and the workpiece surface. Performing UVAG with vibration in the axial direction maintained this characteristic even at the high feed rate used in this study. This is in accordance with observations made by Zhong et al. [44]. The separation of contact between the abrasives and the workpiece results in effective penetration of lubricant, thereby improving the effectiveness of MQL in UVAG.

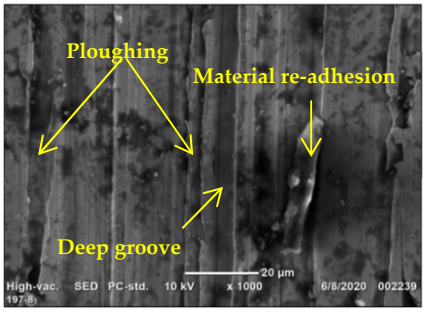

(**a**) SEM Image (1000×)

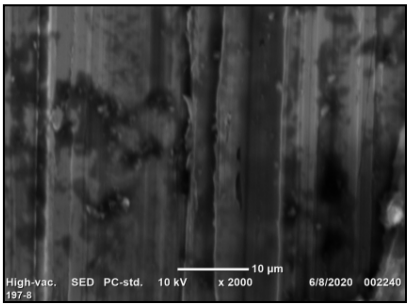

(**b**) SEM Image (2000×)

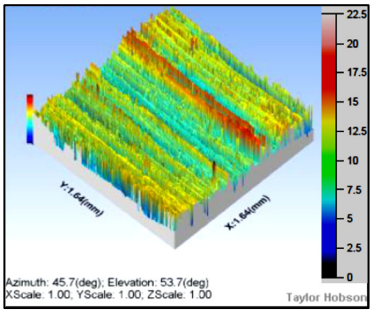

(**c**) 3D Surface Plot

CG_Dry grinding condition

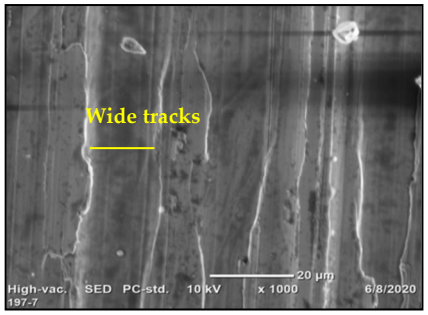

(**d**) SEM Image (1000×)

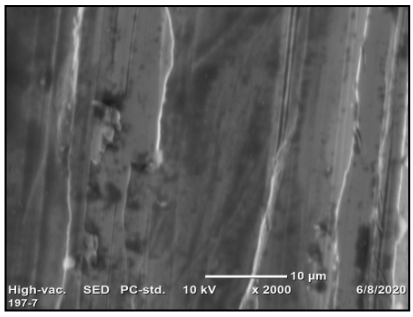

(**e**) SEM Image (2000×)

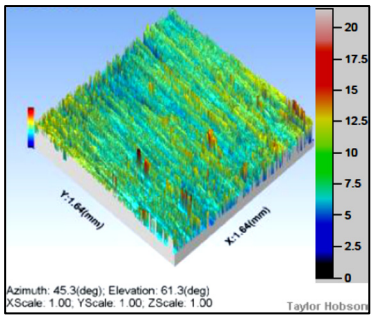

(**f**) 3D Surface Plot

UVAG_Dry grinding condition

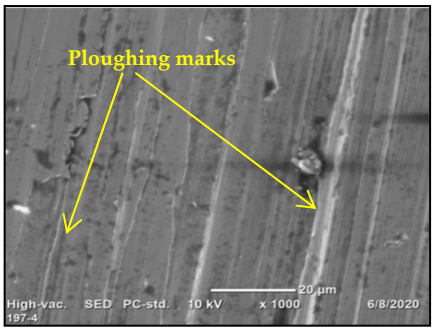

(**g**) SEM Image (1000×)

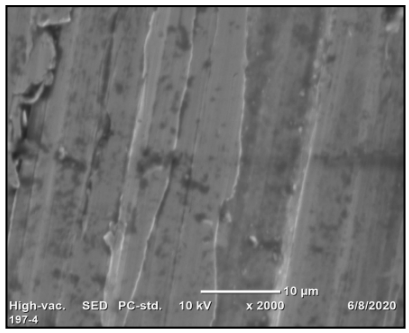

(**h**) SEM Image (2000×)

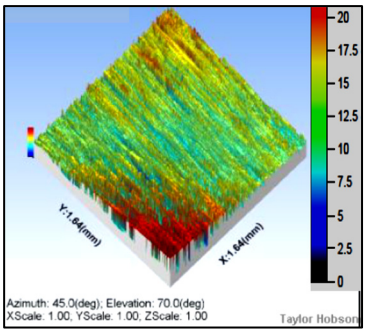

(**i**) 3D Surface Plot

CG_MQL grinding condition

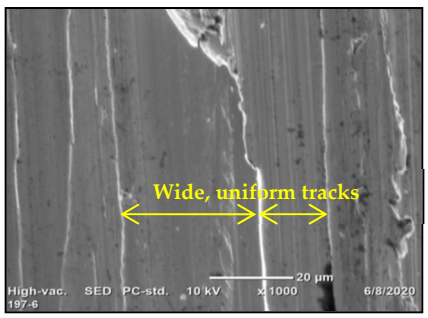

(**j**) SEM Image (1000×)

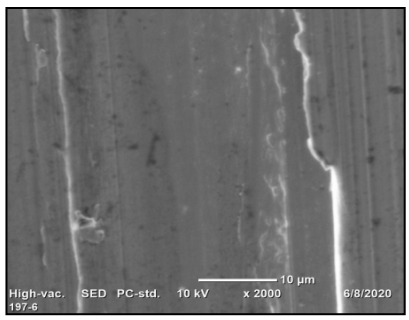

(**k**) SEM Image (2000×)

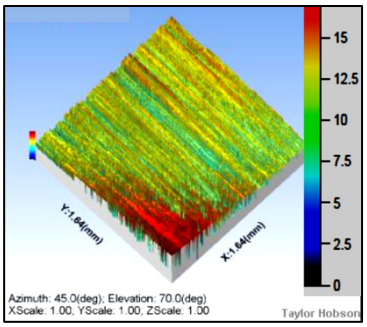

(**l**) 3D Surface Plot

UVAG_MQL grinding condition

Figure 11. Comparison of surface morphologies using SEM and 3D surface plots for CG and UVAG under dry and MQL grinding conditions at vibration amplitude A = 20 µm.

As the cutting action of grits can be enhanced by effective lubrication in UVAG, the surface generated through UVAG_MQL had a significantly improved texture. Hence, it can be concluded that assistance of high frequency vibrations in the axial direction in presence of MQL has the potential to enhance surface quality during grinding of Inconel 718.

4. Statistical Analysis of Grinding Performance

To understand the statistical significance of the factors on the responses, two-way ANOVA was conducted to evaluate the effects of grinding conditions on grinding force and surface roughness. The independent variables were categorized as follows: lubrication condition (two levels: dry and MQL) and amplitude (five levels: 0 µm, 14 µm, 16 µm, 18 µm, and 20 µm, where 0 µm represents CG). Given the experimental design, where grinding is carried out at different amplitudes under each lubrication condition, the amplitude factor was nested within the lubrication factor. This nesting structure allows analysis of how the lubrication condition affects the relationship between the amplitude and the response variables. Hence, it enabled assessment of the main effects for both lubrication and amplitude, as well as the inherent interaction between these factors. The analysis was then performed with grinding forces (F_t and F_n) and surface roughness parameter (R_a) as the responses. Following ANOVA, post-hoc analysis was performed using Fisher's Least Significant Difference (LSD) method to identify specific differences in means between the levels of amplitude under each lubrication condition. For this, CG was considered as the control value, and all deviations were calculated from CG under dry lubrication conditions. This step is essential for understanding the significance of the differences in grinding force and surface roughness, by considering the measured values in conventional grinding in a dry environment as the baseline. For this analysis, box-and-whisker plots are employed to compare the grinding forces and roughness parameter across different conditions, to provide a clear representation of the data distribution and variability. The statistical analysis performed here is in line with the study carried out by Sládek et al. [45], in which ANOVA combined with Fisher LSD post-hoc test was employed to assess the difference in grinding efficiency for various conditions. The results from the analysis are discussed below.

4.1. Statistical Analysis of Grinding Forces

The two-way ANOVA results for normal and tangential forces are presented in Tables 3 and 4, respectively. The analysis revealed significant effects of lubrication conditions and amplitude on the grinding forces. ANOVA indicated a statistically significant difference between the dry and MQL conditions ($p < 0.01$) on the grinding forces F_n and F_t. The results for amplitude (nested within lubrication) also demonstrated significant differences across the various levels ($p < 0.01$). These findings suggest that both lubrication conditions and amplitude substantially influence grinding forces. To further examine specific differences among the amplitude levels under each lubrication condition, post-hoc analysis using Fisher's LSD was conducted. Each amplitude level was compared to conventional grinding (CG) under dry lubrication conditions. The differences in means for grinding forces, *Fn* and *Ft*, shown in Tables 5 and 6, respectively, are statistically significant for all amplitude levels, with *p*-values less than 0.01. The mean differences between UVAG and CG indicate a significant reduction in grinding force, *Fn*, with higher amplitudes. A similar conclusion can be drawn for tangential force, *Ft*. Graphical representations of these differences are illustrated in Figures 12 and 13.

These figures enable visualization of the mean differences between the groups for each pair of conditions being compared. The graphs clearly show that increasing vibration amplitude consistently leads to lower grinding forces. Switching the lubrication condition from dry to MQL in CG significantly reduced grinding forces, as shown by a mean difference of −34.05 in normal grinding force (Fn) between CG under dry and MQL conditions. The introduction of ultrasonic vibrations further reduced grinding forces, with substantial reductions observed across all amplitude levels compared to CG. For instance, mean

differences of −55.13 in F_n and −41.73 in F_t were observed when using UVAG at a 20 µm amplitude under MQL conditions compared to −34.05 and −23.40 when MQL was used in CG.

Table 3. ANOVA for normal grinding force (F_n).

Source	dF	Adj SS	Adj MS	F-Value	*p*-Value
Lubrication	1	5481.0	5481.02	717.12	<0.01
Amplitude (lubrication)	8	3034.7	379.34	49.63	<0.01
Error	20	152.9	7.64		
Total	29	8668.6			

Table 4. ANOVA for tangential grinding force (F_t).

Source	dF	Adj SS	Adj MS	F-Value	*p*-Value
Lubrication	1	3760.34	3760.34	1125.64	<0.01
Amplitude (lubrication)	8	1388.00	173.50	51.94	<0.01
Error	20	66.81	3.34		
Total	29	5215.15			

Table 5. Fisher individual tests for level mean—control mean for normal grinding force (Fn).

Difference of Amplitude (Lubrication) Levels	Difference of Means	Individual 95% CI	T-Value	*p*-Value
UVAG 14 µm (Dry)—CG(Dry)	−14.00	(−18.71, −9.29)	−6.20	<0.01
UVAG 16 µm (Dry)—CG(Dry)	−20.67	(−25.38, −15.96)	−9.16	<0.01
UVAG 18 µm (Dry)—CG(Dry)	−28.33	(−33.04, −23.62)	−12.55	<0.01
UVAG 20 µm (Dry)—CG(Dry)	**−35.14**	(−39.85, −30.43)	−15.57	<0.01
CG(MQL)—CG(Dry)	**−34.05**	(−38.76, −29.34)	−15.08	<0.01
UVAG 14 µm (MQL)—CG(Dry)	−43.27	(−47.97, −38.56)	−19.17	<0.01
UVAG 16 µm (MQL)—CG(Dry)	−48.66	(−53.37, −43.95)	−21.56	<0.01
UVAG 18 µm (MQL)—CG(Dry)	−52.20	(−56.91, −47.49)	−23.12	<0.01
UVAG 20 µm (MQL)—CG(Dry)	**−55.13**	(−59.84, −50.42)	−24.42	<0.01

Table 6. Fisher individual tests for level mean—control mean for tangential grinding force (F_t).

Difference of Amplitude (Lubrication) Levels	Difference of Means	Individual 95% CI	T-Value	*p*-Value
UVAG 14 µm (Dry)—CG(Dry)	−8.10	(−11.21, −4.99)	−5.43	<0.01
UVAG 16 µm (Dry)—CG(Dry)	−12.04	(−15.15, −8.92)	−8.07	<0.01
UVAG 18 µm (Dry)—CG(Dry)	−16.88	(−19.99, −13.77)	−11.31	<0.01
UVAG 20 µm (Dry)—CG(Dry)	**−21.02**	(−24.13, −17.90)	−14.08	<0.01
CG(MQL)—CG(Dry)	**−23.40**	(−26.51, −20.28)	−15.68	<0.01
UVAG 14 µm (MQL)—CG(Dry)	**−31.46**	(−34.58, −28.35)	−21.08	<0.01
UVAG 16 µm (MQL)—CG(Dry)	−34.99	(−38.10, −31.87)	−23.44	<0.01
UVAG 18 µm (MQL)—CG(Dry)	−38.41	(−41.53, −35.30)	−25.74	<0.01
UVAG 20 µm (MQL)—CG(Dry)	**−41.73**	(−44.85, −38.62)	−27.96	<0.01

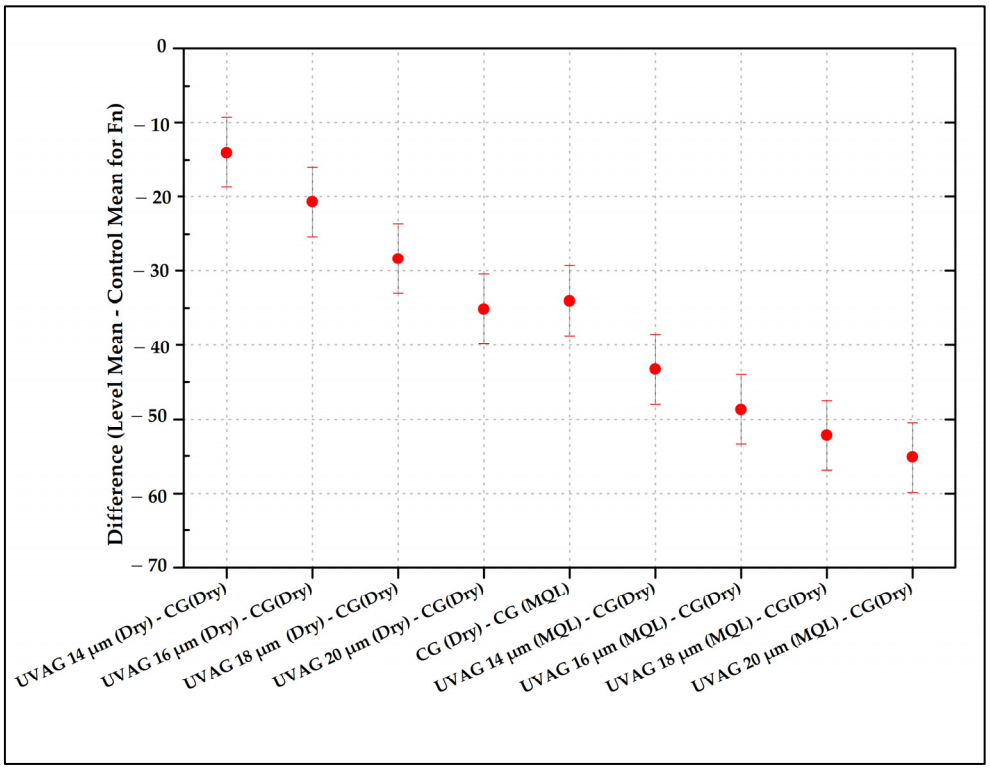

Figure 12. Box-and-whisker plot comparing normal grinding force (F_n) across different conditions using Fisher's LSD method with 95% confidence intervals.

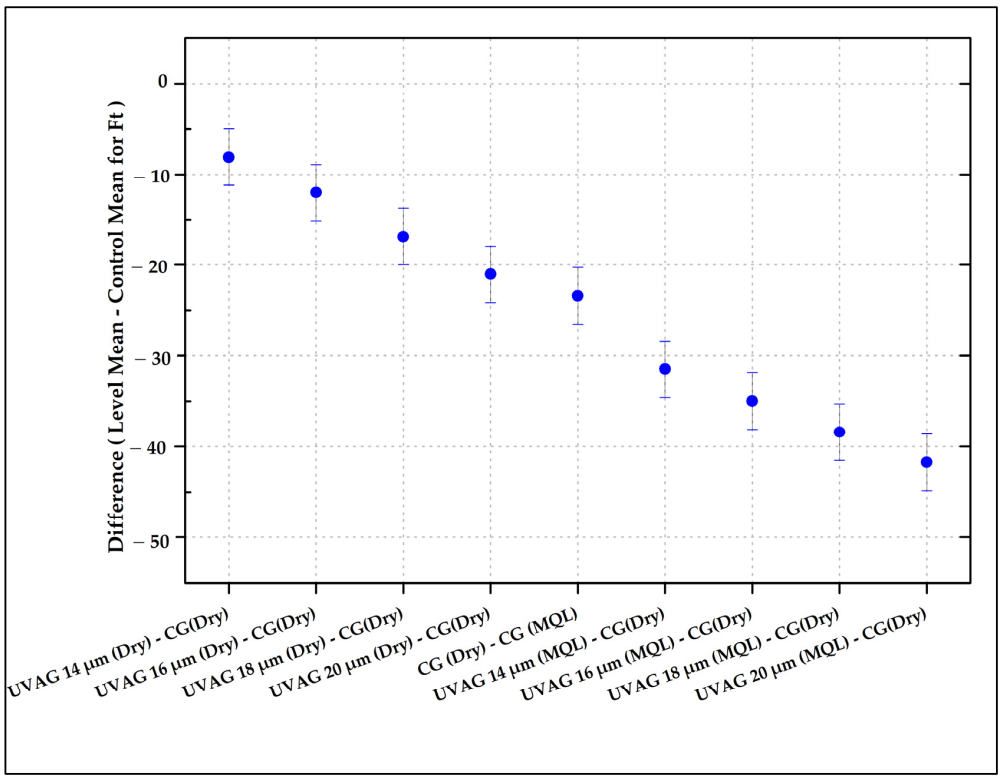

Figure 13. Box-and-whisker plot comparing tangential grinding force (F_t) across different conditions using Fisher's LSD method with 95% confidence intervals.

4.2. Statistical Analysis of Surface Roughness

The ANOVA results for the surface roughness parameter R_a are provided in Table 7. Consistent with the analysis of grinding forces, ANOVA for surface roughness indicated significant effects of both lubrication condition and amplitude. The analysis revealed significant differences between dry and MQL conditions ($p < 0.01$), indicating that lubrication plays a critical role in determining surface finish. The effect of amplitude was also significant, indicating that changes in amplitude affect surface roughness for both lubrication conditions. The Fisher's LSD method results are summarized in Table 8.

Table 7. ANOVA for the surface roughness parameter (R_a).

Source	dF	Adj SS	Adj MS	F-Value	*p*-Value
Lubrication	1	1.7569	1.7569	1112.55	<0.01
Amplitude (lubrication)	8	0.3990	0.0499	31.59	<0.01
Error	20	0.0316	0.0016		
Total	29	2.1876			

Table 8. Fisher Individual Tests for Level Mean—Control Mean for surface roughness (R_a).

Difference of Amplitude (Lubrication) Levels	Difference of Means	Individual 95% CI	T-Value	*p*-Value
UVAG 14 µm (Dry)—CG(Dry)	−0.1180	(−0.1857, −0.0503)	−5.43	<0.01
UVAG 16 µm (Dry)—CG(Dry)	−0.1880	(−0.2557, −0.1203)	−8.07	<0.01
UVAG 18 µm (Dry)—CG(Dry)	−0.2420	(−0.3097, −0.1743)	−11.31	<0.01
UVAG 20 µm (Dry)—CG(Dry)	−0.2670	(−0.3347, −0.1993)	−14.08	<0.01
CG(MQL)—CG(Dry)	−0.4420	(−0.5097, −0.3743)	−15.68	<0.01
UVAG 14 µm (MQL)—CG(Dry)	−0.5580	(−0.6257, −0.4903)	−21.08	<0.01
UVAG 16 µm (MQL)—CG(Dry)	−0.6760	(−0.7437, −0.6083)	−23.44	<0.01
UVAG 18 µm (MQL)—CG(Dry)	−0.7590	(−0.8267, −0.6913)	−25.74	<0.01
UVAG 20 µm (MQL)—CG(Dry)	−0.8000	(−0.8677, −0.7323)	−27.96	<0.01

Each amplitude level was compared against the conventional grinding condition, revealing significant differences across all tested amplitudes. Analysis of the surface roughness data revealed statistically significant differences across all amplitude levels, as shown in Table 8, with *p*-values consistently below 0.01. A substantial reduction in mean surface roughness was observed in UVAG, where R_a decreased with increasing amplitude under both dry and MQL conditions. Figure 14 provides graphical representations of these differences, allowing for easy visualization of the mean differences across conditions. The plot clearly illustrates that increasing vibration amplitude was associated with a significant reduction in surface roughness, underscoring the effectiveness of both MQL lubrication and increased amplitude.

Adopting MQL in CG improves surface roughness significantly, as can be observed from the mean reduction in Ra (−23.40 for Ra when comparing CG in dry vs. MQL). Utilization of UVAG under both dry and MQL conditions led to further improvements in surface roughness. Mean differences of −21.02 and −41.73, respectively, were observed for UVAG at a 20 µm amplitude under dry and MQL conditions compared to CG (Dry). For UVAG, the combination of ultrasonic vibrations and effective lubrication contributed to a smoother surface finish, reducing the roughness significantly. These findings emphasize the importance of lubrication and vibration amplitude settings in achieving optimal surface roughness.

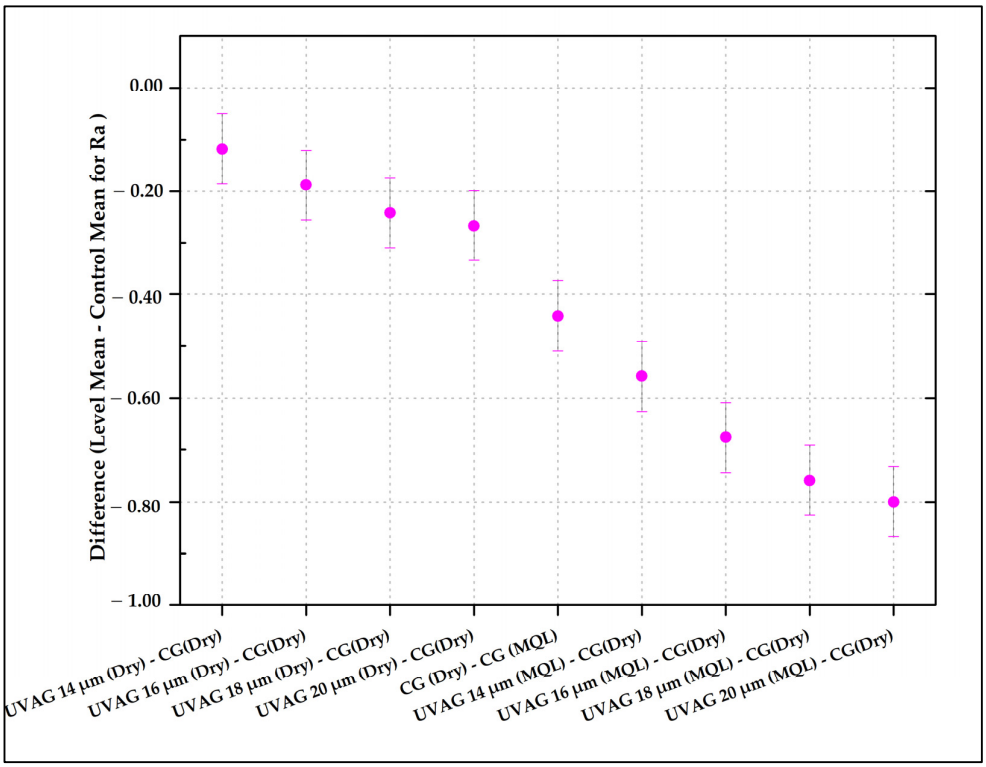

Figure 14. Box-and-whisker plot comparing surface roughness parameter (R_a) across different conditions values using Fisher's LSD method with 95% confidence intervals.

5. Conclusions

In this paper, grinding studies on Inconel 718 with an emphasis on axial UVAG processing were carried out under dry and MQL environments. The samples from UVAG were compared with CG in terms of grinding force, microhardness, residual stress, and surface texture. The key findings of this study are as follows:

1. The application of ultrasonic vibrations significantly reduces both tangential (F_t) and normal (F_n) grinding forces. At a vibration amplitude of 20 µm, F_t was reduced by 33% in UVAG and 44% in UVAG with MQL conditions, while F_n was reduced by 27% under dry conditions and 22% in UVAG with MQL. This reduction in force indicates a more efficient grinding process, resulting in less tool wear and longer tool life.
2. As ultrasonic vibration assistance was imparted to the workpiece in the transverse/axial direction in this study, the axial force F_x recorded by the dynamometer signifies the mechanical action of abrasives in the axial direction. Axial ultrasonic vibrations increase the contact area between abrasives and the workpiece, leading to a reduction in specific energy requirements. The coefficient of friction was observed to be lower in UVAG compared to CG, denoting the effective cutting action of grits and the ease of material removal. This signifies efficient material removal with reduced ploughing and rubbing action in UVAG. As vibration amplitude increases, the specific energy consumed during grinding further decreases, indicating enhanced efficiency.
3. Samples processed with UVAG exhibit compressive residual stress profiles, particularly at higher vibration amplitudes. This indicates the predominance of plastic deformation through the mechanical action of grits and the absence of thermal effects on the workpiece surface. The periodic separation of abrasive contact with the workpiece in UVAG allowed effective lubrication, which enhanced the compressive residual stress.
4. The surface roughness analysis indicates that transitioning from CG to UVAG, along with the use of MQL, significantly enhances surface quality. The surface roughness parameters for UVAG under dry conditions are comparable to those in CG with

MQL, with a notable 51% reduction in R_a at a 20 µm amplitude. In terms of 3D roughness parameters, both average roughness (S_a) and root mean square roughness (S_q) showed marked reductions under UVAG conditions compared to CG, with the best results observed in UVAG_MQL scenarios. The negative skewness (Ssk) and reduced kurtosis (Sku) in UVAG suggest a smoother surface profile with fewer sharp peaks, making UVAG and MQL highly effective for improving the surface finish of Inconel 718 in high-performance applications.

5. SEM imaging revealed that UVAG produces surfaces with fewer ploughing marks and more uniform grain tracks, transitioning from the continuous abrasive path seen in CG to an elliptical trace in UVAG. Analysis of the 3D surface profile further demonstrated improvements in kurtosis and skewness, indicating a plateaued surface with reduced sharp peaks and troughs. This suggests a more consistent texture, contributing to enhanced performance in subsequent applications.
6. The statistical analyses conducted in this study revealed important insights into the dynamics of grinding under different conditions. ANOVA followed by Fischer's LSD test was employed to analyze the significance of the results. The statistical parameters also indicate that increasing vibration amplitude consistently reduces grinding forces, with higher amplitudes yielding greater reductions. The analysis also revealed that MQL improves surface roughness, while the combination of UVAG and effective lubrication leads to substantial enhancements in surface quality. Additionally, switching from dry to MQL lubrication significantly lowers grinding forces and surface roughness, and ultrasonic vibrations further enhance this effect.

In summary, both changing the grinding condition from dry to MQL and adopting UVAG as a technique significantly enhance grinding performance. The results obtained in this study reaffirm the potential of UVAG as an efficient and sustainable grinding method for Inconel 718 when appropriate processing conditions are identified. This study demonstrates that UVAG can improve machining efficiency by significantly reducing grinding forces and specific energy consumption. The superior surface finish and generation of compressive residual stress due to vibration assistance in UVAG are particularly beneficial in high performance applications, and the impact on mechanical properties requires attention. Furthermore, UVAG's efficiency in reducing grinding forces and energy consumption translates into lower operational costs. The improved efficiency in material removal makes UVAG a more eco-friendly option compared to traditional grinding methods. Future research can focus on utilizing the versatility of UVAG to optimize the grinding process for different materials and applications, while also exploring further economic and ecological benefits.

Author Contributions: Conceptualization, S.D.; methodology, S.D. and P.C.; validation, P.C., A.P. and A.B.; formal analysis, S.D.; investigation, S.D.; resources, J.J. and J.P.; data curation, S.D. and A.P.; writing—original draft preparation, S.D.; writing—review and editing, P.C.; visualization, S.D. and A.P.; supervision, P.C. and A.B.; project administration, P.C.; funding acquisition, A.B. All authors have read and agreed to the published version of the manuscript.

Funding: This research received no external funding.

Data Availability Statement: Data are contained within the article.

Acknowledgments: The authors gratefully acknowledge Advanced Material Processing Laboratory at Vellore Institute of Technology for providing access to the labs and instrumentation critical to this research work.

Conflicts of Interest: The authors declare no conflicts of interest.

References

1. Battaglia, F.; Arie, M.; Zhang, X.; Ohadi, M.; Shooshtari, A. Experimental Characterization of an Additively Manufactured Inconel 718 Heat Exchanger for High-Temperature Applications. *Energies* **2023**, *16*, 4156. [CrossRef]
2. Marques, A.; Guimarães, B.; Bartolomeu, F.; Miranda, G.; Silva, F.S.; Carvalho, O. Multi-Material Inconel 718—Aluminium Parts Targeting Aerospace Applications: A Suitable Combination of Low-Weight and Thermal Properties. *Opt. Laser Technol.* **2023**, *158*, 108913. [CrossRef]
3. Meng, G.; Gong, Y.; Zhang, J.; Ren, Q.; Zhao, J. Microstructure Effect on the Machinability Behavior of Additive and Conventionally Manufactured Inconel 718 Alloys. *J. Mater. Process. Technol.* **2024**, *324*, 118228. [CrossRef]
4. Jeyapandiarajan, P.; Anthony Xavior, M. Evaluating the Machinability of Inconel 718 under Different Machining Conditions. *Procedia Manuf.* **2019**, *30*, 253–260. [CrossRef]
5. Xavior, M.A.; Ranganathan, N.; Ashwath, P. Effect of Recast Layer on the Low Cycle Fatigue Life of Electric Discharge Machined Inconel 718. *Mater. Today Proc.* **2018**, *5*, 12666–12672. [CrossRef]
6. Xavior, M.A.; Ashwath, P.; Ali, H.; Moideen, A.; Banu, P.; Raneez, M.; Sancylal, S. Effect of Recast Layer Thickness on the Mechanical Characteristics of INCONEL 718 Machined by Spark EDM Process. *Mater. Today Proc.* **2018**, *5*, 8249–8255. [CrossRef]
7. Dai, C.-W.; Ding, W.-F.; Zhu, Y.-J.; Xu, J.-H.; Yu, H.-W. Grinding Temperature and Power Consumption in High Speed Grinding of Inconel 718 Nickel-Based Superalloy with a Vitrified CBN Wheel. *Precis. Eng.* **2018**, *52*, 192–200. [CrossRef]
8. Curtis, D.; Krain, H.; Winder, A.; Novovic, D. Impact of Grinding Wheel Specification on Surface Integrity and Residual Stress When Grinding Inconel 718. *Proc. Inst. Mech. Eng. B J. Eng. Manuf.* **2021**, *235*, 1668–1681. [CrossRef]
9. Martins, H.; Puga, H. Ultrasonic Assisted Machining Overview: Accessing Feasibility and Overcoming Challenges for Milling Applications. *Metals* **2023**, *13*, 908. [CrossRef]
10. Venkatesan, K.; Ramanujam, R.; Kuppan, P. Laser Assisted Machining of Difficult to Cut Materials: Research Opportunities and Future Directions—A Comprehensive Review. *Procedia Eng.* **2014**, *97*, 1626–1636. [CrossRef]
11. Saxena, K.K.; Bellotti, M.; Qian, J.; Reynaerts, D.; Lauwers, B.; Luo, X. Overview of Hybrid Machining Processes. In *Hybrid Machining*; Elsevier: Amsterdam, The Netherlands, 2018; pp. 21–41.
12. Cao, Y.; Zhao, B.; Ding, W.; Wu, J.; Jia, X.; Zhang, J.; Das, R. Intermittent Cutting Behavior and Grinding Force Model in Ultrasonic Vibration-Assisted Grinding K4002 Nickel-Based Superalloy. *Int. J. Adv. Manuf. Technol.* **2024**, *131*, 3085–3102. [CrossRef]
13. Chaudhari, A.; Sharma, A.; Yusufzai, M.Z.K.; Vashista, M. The Grindability Performance and Measurement of Surface Functional Parameter Capabilities of Difficult-to-Machine Tool Steel under Tangential Ultrasonic-Vibration-Assisted Dry Grinding. *Mach. Sci. Technol.* **2023**, *27*, 268–291. [CrossRef]
14. Ibrahim, E.E.; Checkley, M.; Chen, X.; Sharp, M.; Liang, W.; Yuan, S.; Batako, A.D.L. Process Performance of Low Frequency Vibratory Grinding of Inconel 718. *Procedia Manuf.* **2019**, *30*, 530–535. [CrossRef]
15. Zhao, B.; You, H.; Miao, Q.; Ding, W.; Qian, N.; Xu, J. Surface Integrity Characterization of Third-Generation Nickel-Based Single Crystal Blade Tenons after Ultrasonic Vibration-Assisted Grinding. *Chin. J. Aeronaut.* **2024**. [CrossRef]
16. Tawakoli, T.; Azarhoushang, B.; Rasifard, A. Wear Behavior of a Vitrified Bond CBN Wheel by Ultrasonic-Assisted Creep Feed Profile Grinding of Inconel 718. *Adv. Mat. Res.* **2011**, *325*, 122–127. [CrossRef]
17. Li, S.; Wu, Y.; Nomura, M. Effect of Grinding Wheel Ultrasonic Vibration on Chip Formation in Surface Grinding of Inconel 718. *Int. J. Adv. Manuf. Technol.* **2016**, *86*, 1113–1125. [CrossRef]
18. Molaie, M.M.; Akbari, J.; Movahhedy, M.R. Ultrasonic Assisted Grinding Process with Minimum Quantity Lubrication Using Oil-Based Nanofluids. *J. Clean. Prod.* **2016**, *129*, 212–222. [CrossRef]
19. Rabiei, F.; Rahimi, A.R.; Hadad, M.J. Performance Improvement of Eco-Friendly MQL Technique by Using Hybrid Nanofluid and Ultrasonic-Assisted Grinding. *Int. J. Adv. Manuf. Technol.* **2017**, *93*, 1001–1015. [CrossRef]
20. Das, S.; Anil, L.; Pandivelan, C. Design and Development of an Ultrasonic Stack Assembly for Ultrasonic Vibration Assisted Grinding. *Mater. Today Proc.* **2021**, *46*, 8778–8782. [CrossRef]
21. Ding, K.; Fu, Y.; Su, H.; Xu, H.; Cui, F.; Li, Q. Experimental Studies on Matching Performance of Grinding and Vibration Parameters in Ultrasonic Assisted Grinding of SiC Ceramics. *Int. J. Adv. Manuf. Technol.* **2017**, *88*, 2527–2535. [CrossRef]
22. Yang, Z.; Zhu, L.; Ni, C.; Ning, J. Investigation of Surface Topography Formation Mechanism Based on Abrasive-Workpiece Contact Rate Model in Tangential Ultrasonic Vibration-Assisted CBN Grinding of ZrO_2 Ceramics. *Int. J. Mech. Sci.* **2019**, *155*, 66–82. [CrossRef]
23. Abdullah, A.; Farhadi, A.; Pak, A. Ultrasonic-Assisted Dry Creep-Feed Up-Grinding of Superalloy Inconel738LC. *Exp. Mech.* **2012**, *52*, 843–853. [CrossRef]
24. Das, S.; Pandivelan, C.; Reddy, M.S.S.M.; Kesava, D.; Avinash, Y.A.V. Optimisation of Ultrasonic Assisted Grinding of Inconel 718 Using Grey Relational Analysis. *IP Conf. Proc.* **2021**, *2341*, 040019.
25. Yao, C.F.; Jin, Q.C.; Huang, X.C.; Wu, D.X.; Ren, J.X.; Zhang, D.H. Research on Surface Integrity of Grinding Inconel718. *Int. J. Adv. Manuf. Technol.* **2013**, *65*, 1019–1030. [CrossRef]
26. Wang, Y.; Lin, B.; Cao, X.; Wang, S. An Experimental Investigation of System Matching in Ultrasonic Vibration Assisted Grinding for Titanium. *J. Mater. Process. Technol.* **2014**, *214*, 1871–1878. [CrossRef]
27. Balan, A.S.S.; Vijayaraghavan, L.; Krishnamurthy, R. Minimum Quantity Lubricated Grinding of Inconel 751 Alloy. *Mater. Manuf. Process.* **2013**, *28*, 430–435. [CrossRef]

28. Cao, Y.; Zhao, B.; Ding, W.; Liu, Y.; Wang, L. On the Tool Wear Behavior during Ultrasonic Vibration-Assisted Form Grinding with Alumina Wheels. *Ceram. Int.* **2021**, *47*, 26465–26474. [CrossRef]
29. Shen, J.Y.; Wang, J.Q.; Jiang, B.; Xu, X.P. Study on Wear of Diamond Wheel in Ultrasonic Vibration-Assisted Grinding Ceramic. *Wear* **2015**, *332–333*, 788–793. [CrossRef]
30. Marinescu, I.D.; Hitchiner, M.P.; Uhlmann, E.; Rowe, W.B.; Inasaki, I. *Handbook of Machining with Grinding Wheels*; CRC Press: Boca Raton, FL, USA, 2006; ISBN 9780429136115.
31. Zhong, Z.-W. Advanced Polishing, Grinding and Finishing Processes for Various Manufacturing Applications: A Review. *Mater. Manuf. Process.* **2020**, *35*, 1279–1303. [CrossRef]
32. Chakule, R.R.; Chaudhari, S.S.; Talmale, P.S. Evaluation of the Effects of Machining Parameters on MQL Based Surface Grinding Process Using Response Surface Methodology. *J. Mech. Sci. Technol.* **2017**, *31*, 3907–3916. [CrossRef]
33. Li, Y.; Jiao, L.; Liu, Y.; Tian, Y.; Qiu, T.; Zhou, T.; Wang, X.; Zhao, B. Study on a Novel Strategy for High-Quality Grinding Surface Based on the Coefficient of Friction. *Lubricants* **2023**, *11*, 351. [CrossRef]
34. Strunk, R.; Borchers, F.; Clausen, B.; Heinzel, C. Influence of Subsequently Applied Mechanical and Thermal Loads on Surfaces Ground with Mechanical Main Impact. *Materials* **2021**, *14*, 2386. [CrossRef] [PubMed]
35. Zhong, Z.; Ramesh, K.; Yeo, S.H. Grinding of Nickel-Based Super-Alloys and Advanced Ceramics. *Mater. Manuf. Process.* **2001**, *16*, 195–207. [CrossRef]
36. Maroju, N.K.; Jin, X. Effects of Vibration Assistance on Surface Residual Stress in Grinding of Ti6Al4V Alloy. *Procedia Manuf.* **2017**, *10*, 171–182. [CrossRef]
37. Naskar, A.; Singh, B.B.; Choudhary, A.; Paul, S. Effect of Different Grinding Fluids Applied in Minimum Quantity Cooling-Lubrication Mode on Surface Integrity in CBN Grinding of Inconel 718. *J. Manuf. Process.* **2018**, *36*, 44–50. [CrossRef]
38. Wang, J.; Xu, J.; Wang, X.; Zhang, X.; Song, X.; Chen, X. A Comprehensive Study on Surface Integrity of Nickel-Based Superalloy Inconel 718 under Robotic Belt Grinding. *Mater. Manuf. Process.* **2019**, *34*, 61–69. [CrossRef]
39. Xu, N.; Dong, Z.; Kang, R.; Bao, Y.; Du, H.; Shan, K.; Guo, D.; Wang, Y. Surface Microstructure Evolution Analysis of Inconel 718 during Ultrasonic Vibration-Assisted Grinding Using FEM. *J. Manuf. Process.* **2024**, *127*, 631–644. [CrossRef]
40. Thakur, A.; Gangopadhyay, S. State-of-the-Art in Surface Integrity in Machining of Nickel-Based Super Alloys. *Int. J. Mach. Tools Manuf.* **2016**, *100*, 25–54. [CrossRef]
41. de Souza Ruzzi, R.; de Paiva, R.L.; da Silva, L.R.R.; Abrão, A.M.; Brandão, L.C.; da Silva, R.B. Comprehensive Study on Inconel 718 Surface Topography after Grinding. *Tribol. Int.* **2021**, *158*, 106919. [CrossRef]
42. Gu, G.; Wang, D.; Wu, S.; Zhou, S.; Zhang, B. Research Status and Prospect of Ultrasonic Vibration and Minimum Quantity Lubrication Processing of Nickel-Based Alloys. *Intell. Sustain. Manuf.* **2024**, *1*, 10006. [CrossRef]
43. Sedlaček, M.; Podgornik, B.; Vižintin, J. Correlation between Standard Roughness Parameters Skewness and Kurtosis and Tribological Behaviour of Contact Surfaces. *Tribol. Int.* **2012**, *48*, 102–112. [CrossRef]
44. Zhong, Z.W.; Yang, H.B. Development of a Vibration Device for Grinding with Microvibration. *Mater. Manuf. Process.* **2004**, *19*, 1121–1132. [CrossRef]
45. Sládek, V.; Hora, M.; Farkašová, K.; Rocek, T.R. Impact of Grinding Technology on Bilateral Asymmetry in Muscle Activity of the Upper Limb. *J. Archaeol. Sci.* **2016**, *72*, 142–156. [CrossRef]